LANGMUIR

pubs.acs.org/Langmuir Article

Photoelectrochemical Enzyme Biosensor Based on TiO_2 Nanorod/TiO_2 Quantum Dot/Polydopamine/Glucose Oxidase Composites with Strong Visible-Light Response

Jinxin Ma, Miaomiao Zhang, Wen Su, Baiqiang Wu, Zhuo Yang, Xiaohong Wang, Bin Qiao, Hua Pei, Jinchun Tu, Delun Chen,* and Qiang Wu*

Cite This: *Langmuir* 2022, 38, 751−761 Read Online

ACCESS | Metrics & More | Article Recommendations | Supporting Information

ABSTRACT: Although photoelectrochemical (PEC) enzyme biosensors based on visible-light detection would have a high practical value, their development has been limited by the weak visible-light response of available photoactive substrates. Here, to enhance the visible-light response of a photoelectric substrate, a TiO_2 nanorods (NRs)/TiO_2 quantum dots (QDs)/polydopamine (PDA)/glucose oxidase nanocomposite was prepared *via* hydrothermal synthesis, followed by photopolymerization. TiO_2 QDs with strong light absorption and excellent photocatalytic activity were introduced between the TiO_2 NRs and the PDA. An efficient electron transport interface that formed as a result of the combination of the TiO_2 NRs, TiO_2 QDs, and the PDA could not only transfer electrons quickly and orderly, but also substantially improve the response of the TiO_2 NRs under visible light. Through a series glucose detection, a sensor based on the nanocomposite was found to exhibit superior sensing performance under visible light with a sensitivity of 4.63 μA mM^{-1} cm^{-2}, a linear response over the concentration 0.1−4 mM, and a detection limit of 8.16 μM. This work proposes a biosensor that can detect under visible light, thereby expanding the application range of PEC enzyme biosensors.

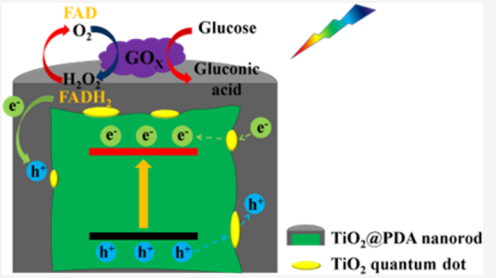

INTRODUCTION

Photoelectrochemical (PEC) enzyme biosensors have been widely used in biological analysis and detection because of their fast response, low cost, low background interference, and high sensitivity.[1,2] Most previous works related to PEC enzyme biosensors have been focused on the UV excitation stage. On the one hand, UV can easily deactivate biomolecules and make the sensor useless. On the other hand, high-energy UV easily triggers side reactions among the substances in the detection system, which will affect the detection results.[3,4] Therefore, the development of PEC enzyme biosensors excited by visible light is important.

TiO_2 nanorods (NRs) are the most commonly used substrates in PEC enzyme biosensors because of their advantages of low preparation cost, nontoxicity, and high specific surface area.[5] However, because TiO_2 has a wide band gap (~3.2 eV), it exhibits no response under visible light and is only excited by UV light with a wavelength <387 nm; the application of traditional TiO_2 materials in the field of visible-light PEC enzyme biosensors has consequently been greatly restricted.[6] Recently, to improve the response of TiO_2 under visible light and expand its application in PEC enzyme biosensors, researchers have investigated strategies such as dye sensitization,[7] metal doping,[8] and incorporation with narrow band gap semiconductors.[9,10] However, some technical problems, such as complicated preparation methods, low doping efficiency, and heavy-metal ion pollution, have restricted the development of PEC enzyme biosensors based on visible-light-responsive TiO_2. However, these problems can be mitigated by loading materials that can improve the light absorption efficiency and biocompatibility of TiO_2.[11] TiO_2 quantum dots (QDs) are zero-dimensional nanomaterials that feature a small particle size, high catalytic activity, and large specific surface area, which impart them with strong light absorbing ability and excellent photocatalytic activity. Most importantly, TiO_2 QDs can be intimately combined with TiO_2 NRs through *in situ* growth, resulting in a material that inhibits electron−hole recombination in a photoelectric reaction, thereby improving the photoelectric response of TiO_2 NRs under visible light.[12,13] Therefore, TiO_2 QDs can be loaded on TiO_2 NRs to improve the response of PEC enzyme biosensors under visible light. In addition, given the biocompatibility requirements of enzymatic biosensors, loading of biologically active substances is necessary. Polydopamine (PDA) exhibits good biocompatibility, high adhesive strength, and a wide

Received: October 14, 2021
Revised: December 21, 2021
Published: January 4, 2022

https://doi.org/10.1021/acs.langmuir.1c02741
Langmuir 2022, 38, 751−761

Scheme 1. Process Used to Fabricate the TiO_2 NRs/TiO_2 QDs/PDA Electrode

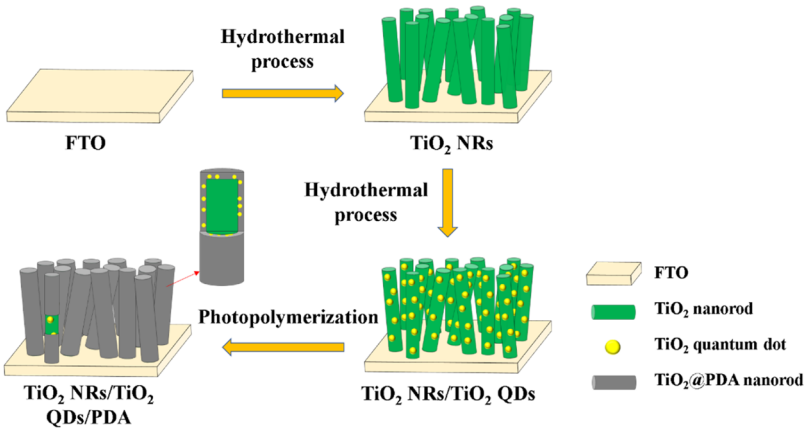

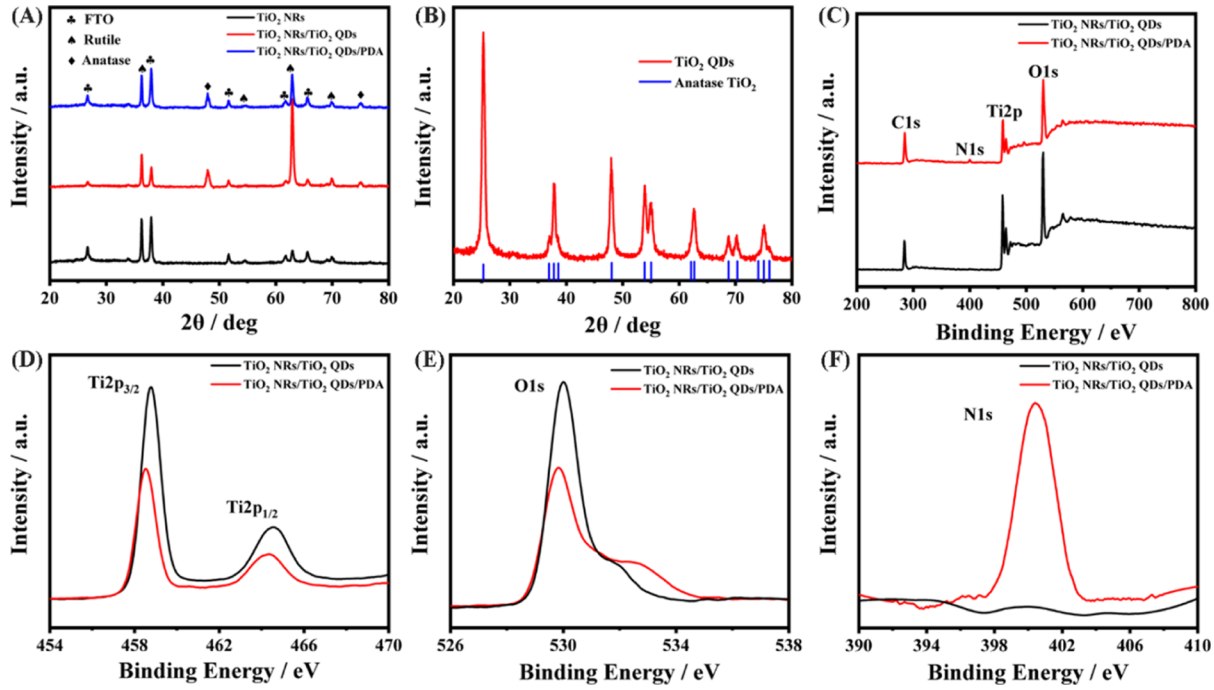

Figure 1. (A) XRD patterns of the TiO_2 NRs (black line), TiO_2 NRs/TiO_2 QDs (red line), and TiO_2 NRs/TiO_2 QDs/PDA (blue line) and (B) TiO_2 QDs (the vertical blue lines indicate the peaks corresponding to the PDF data for anatase). (C) XPS full spectrum and (D) Ti 2*p*, (E) O 1*s*, and (F) N 1*s* high-resolution spectra of the TiO_2 NRs/TiO_2 QDs and TiO_2 NRs/TiO_2 QDs/PDA.

absorption range and has therefore often been used to modify the photoelectrochemically active material.[14,15]

Herein, we developed a PEC enzyme biosensor based on PDA-assisted visible-light excitation and used the device to detect glucose. TiO_2 QDs were grown uniformly *in situ* on the surface of TiO_2 NRs through a simple hydrothermal reaction. The *in situ* growth of TiO_2 QDs not only reduced the bulk defects of the TiO_2 NRs but also formed a heterojunction with them *via* the strong bonding force to reduce the electron−hole recombination efficiency. Moreover, photopolymerization of PDA on the surface of the material induced polymer chain conjugation, which promoted light-induced charge separation and further broadened the absorption of the material in the visible-light range. Because of the long-lasting stability and presence of reactive groups, the PDA could control the electron transmission path of the TiO_2 QDs and introduce reactive groups to form a coupled conjugate structure with TiO_2 QDs, resulting in the formation of an efficient transmission channel. Glucose detection experiments revealed that the obtained TiO_2 NRs/TiO_2 QDs/PDA/GOx (GOx = glucose oxidase) biosensor shows excellent response to glucose with the sensitivity of 4.63 μA mM^{-1} cm^{-2}, a linear response over the concentration 0.1−4 mM, and a detection limit of 8.16 μM. In summary, the introduction of TiO_2 QDs between TiO_2 NRs and PDA greatly improved the response of the material under visible light, providing a new alternative material for use in biosensors.

EXPERIMENTAL SECTION

Synthesis of TiO_2 NRs. TiO_2 NRs were grown on fluorine-doped tin oxide (FTO) glass using the hydrothermal method reported by Liu and Aydil.[16] First, the FTO glass was sequentially cleaned in isopropyl alcohol, acetone, and ultrapure water ultrasonically for 20 min. Second, 10 mL of hydrochloric acid was added to 10 mL ultrapure water, and the resultant solution was stirred for 10 min. Four hundred microliters of titanium isopropoxide was then added,

https://doi.org/10.1021/acs.langmuir.1c02741
Langmuir 2022, 38, 751−761

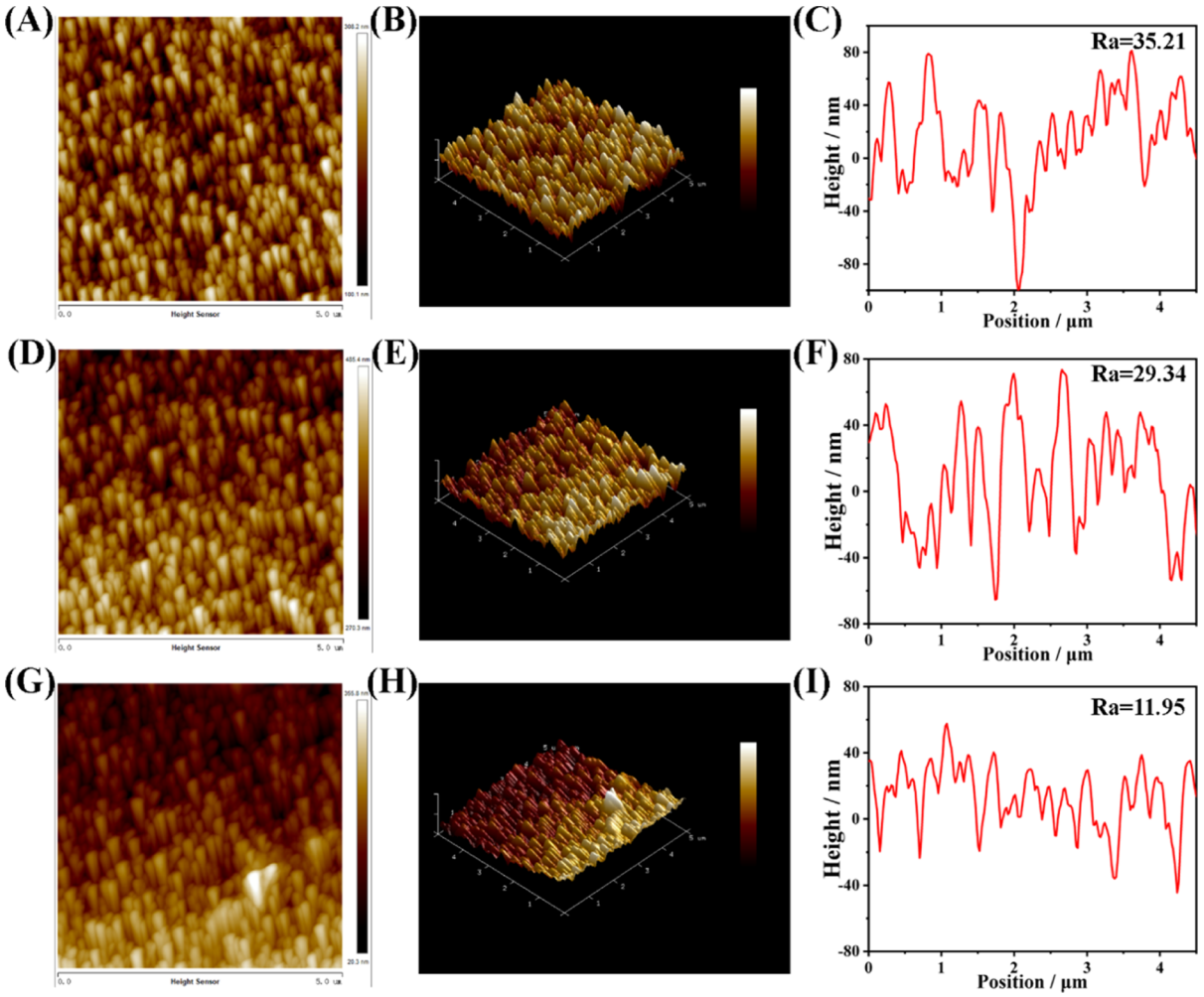

Figure 2. 2D, 3D, and height profile images of (A–C) TiO_2 NRs, (D–F) TiO_2 NRs/TiO_2 QDs, and (G–I) TiO_2 NRs/TiO_2 QDs/PDA electrodes, as obtained by AFM analysis.

and the mixture was stirred vigorously for ~30 min. The FTO glass was then placed face down against the wall at an angle in a Teflon-lined container (30 mL), and the prepared solution was added. The Teflon-lined container was inserted into a stainless-steel autoclave, which was placed in an oven and heated for 4 h at 150 °C; then, the autoclave was allowed to cool to room temperature naturally. Afterward, the FTO glass was taken and rinsed several times with ethanol and ultrapure water. Finally, the dried samples were annealed at 450 °C for 4 h at a heating rate of 2 °C/min.

Synthesis of TiO_2 NRs/TiO_2 QDs. The TiO_2 NRs/TiO_2 QDs were prepared by a simple hydrothermal approach. First, 5.8 g of hexadecyl trimethyl ammonium bromide ($C_{19}H_{42}BrN$) was added to a mixed solution of 60 mL of *n*-hexane and 10 mL of *n*-pentanol. Ten milliliters of ultrapure water was then slowly added, and the resultant solution was stirred vigorously for 10 min. Eight hundred microliters of titanium(III) trichloride was then added to the solution, and the resultant mixture was stirred for 10 min. Afterward, 11.4 mL of acetic acid was added dropwise to the mixed solution and stirred until it was smooth, resulting in the formation of a pale-pink oil-and-water emulsion. Thirty milliliters of the prepared emulsion was transferred to a Teflon-lined container (50 mL), and FTO glass with TiO_2 NRs was placed face down against the Teflon wall at an angle. The Teflon-lined container was transferred to a stainless-steel autoclave, which was placed in an oven and heated for 3 h at 200 °C; then, the autoclave was allowed to cool to room temperature naturally. Finally, the FTO glass was removed from the autoclave and then repeatedly washed with ethanol and ultrapure water to remove surfactants and other impurities.

Fabrication of the PEC Electrode. One hundred milligrams of dopamine hydrochloride was added to 50 mL of phosphate-buffered saline (PBS) solution (pH = 6.0), and the resultant solution was slightly stirred. The TiO_2 NRs/TiO_2 QDs substrate obtained was placed in the solution and irradiated under a UV lamp for 4 h. The prepared TiO_2 NRs/TiO_2 QDs/PDA electrode was washed with ultrapure water and stored in a refrigerator at 4 °C for 30 min. The electrode construction process is shown in Scheme 1. Afterward, 20 μL of GOx and 10 μL of chitosan solution were added dropwise to the surface of the TiO_2 NRs/TiO_2 QDs/PDA electrode, which was subsequently placed in a refrigerator at 4 °C for further use.

RESULTS AND DISCUSSION

Characterization of the TiO_2 NRs/TiO_2 QDs/PDA Electrode. To investigate the crystal structure of the electrode material, the materials synthesized in the present work were analyzed by X-ray diffraction (XRD, Figure 1A). The diffraction peaks corresponding to the black curve are well consistent with the diffraction peaks of rutile TiO_2[17] specified in JCPDS no. 02-0494, indicating that the TiO_2 NRs prepared in the present work was pure rutile phase. Compared with the XRD pattern of the TiO_2 NRs, that of the TiO_2 NRs/TiO_2 QDs (Figure 1A) showed two new peaks at 47.96 and 74.99°, which are the characteristic peaks of anatase TiO_2; the appearance of these peaks thus implies the presence of anatase in the TiO_2 QDs. To further investigate the crystal structure of

https://doi.org/10.1021/acs.langmuir.1c02741
Langmuir 2022, 38, 751–761

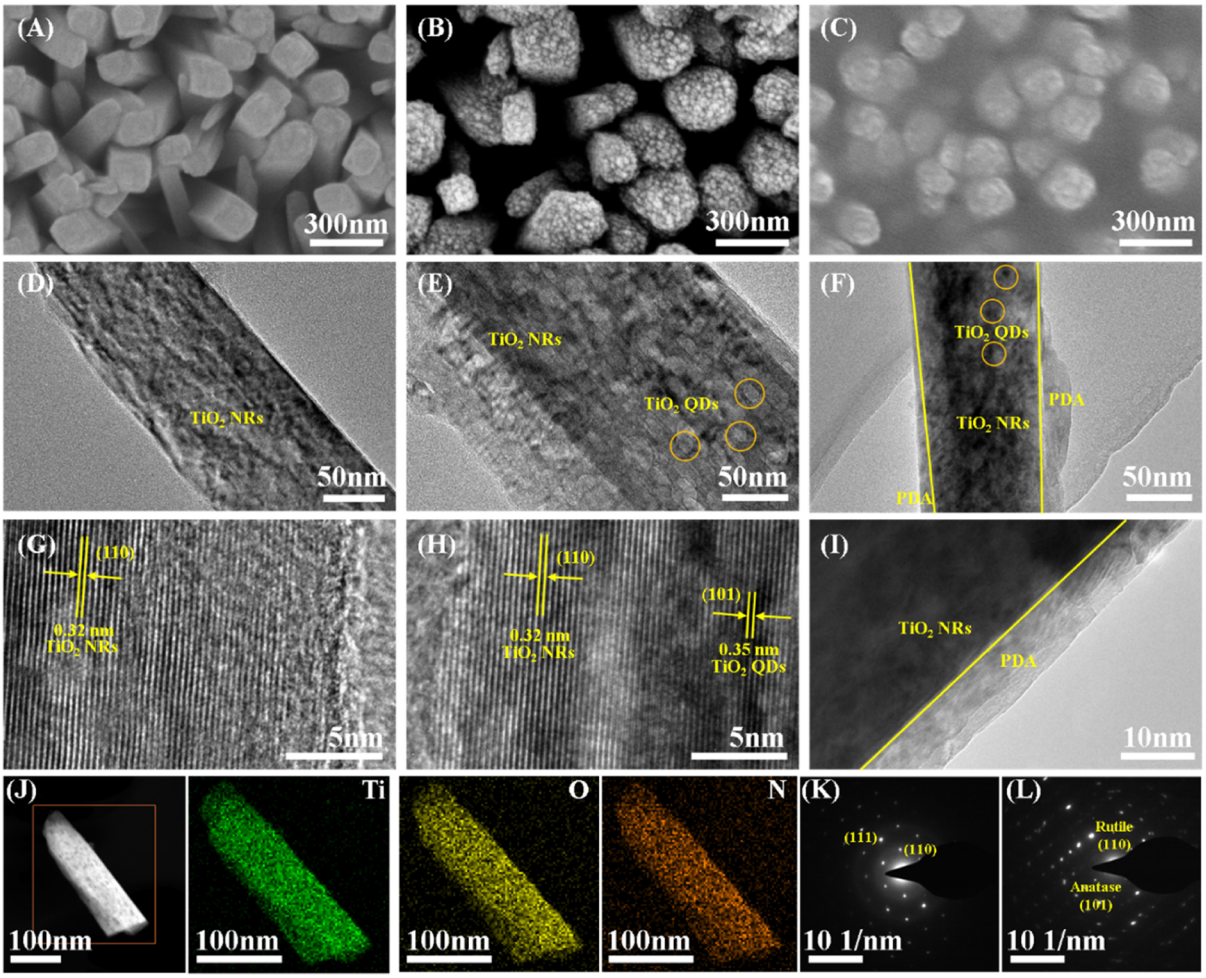

Figure 3. SEM images of the (A) TiO_2 NRs, (B) TiO_2 NRs/TiO_2 QDs, and (C) TiO_2 NRs/TiO_2 QDs/PDA. TEM images of the (D) TiO_2 NRs, (E) TiO_2 NRs/TiO_2 QDs, and (F) TiO_2 NRs/TiO_2 QDs/PDA. HRTEM images of the (G) TiO_2 NRs, (H) TiO_2 NRs/TiO_2 QDs, and (I) TiO_2 NRs/TiO_2 QDs/PDA. (J) Energy-dispersive X-ray spectroscopy mapping images of the TiO_2 NRs/TiO_2 QDs/PDA. SAED patterns of the (K) TiO_2 NRs and (L) TiO_2 NRs/TiO_2 QDs.

the TiO_2 QDs, the XRD pattern of the TiO_2 QDs was recorded alone. The diffraction peaks of the TiO_2 QDs were well consistent with the anatase TiO_2[18] diffraction peaks in JCPDS no. 21-1272 (Figure 1B), indicating that the TiO_2 QDs prepared in the present work have a pure anatase phase with excellent crystallinity. The blue curve (Figure 1A) shows the XRD pattern of the TiO_2 NRs/TiO_2 QDs/PDA electrode, where the diffraction peak positions are basically consistent with those of the TiO_2 NRs/TiO_2 QDs electrode; no new peaks were observed. These results indicate that the PDA synthesized by photopolymerization may be an amorphous compound that cannot be characterized by XRD analysis.

To further confirm the elemental chemical states and surface chemical compositions of the as-prepared electrodes, X-ray photoelectron spectroscopy (XPS) was used to analyze the synthesized electrode materials and the obtained spectra were compared with those for the TiO_2 NRs/TiO_2 QDs electrode. Figure 1C shows the XPS full spectrum of the TiO_2 NRs/TiO_2 QDs electrode (black line) and the TiO_2 NRs/TiO_2 QDs/PDA electrode (red line). Peaks of C *1s*, N *1s*, Ti *2p*, and O *1s* are observed in the spectrum of the TiO_2 NRs/TiO_2 QDs/PDA electrode, whereas peaks of C *1s*, Ti *2p*, and O *1s* are observed in the spectrum of the TiO_2 NRs/TiO_2 QDs. Compared with the TiO_2 NRs/TiO_2 QDs electrode, the Ti *2p* and O *1s* peaks in the spectrum of the TiO_2 NRs/TiO_2 QDs/PDA electrode are substantially less intense; in addition, a new peak N *1s* appears in the spectrum. This was because the successful loading of the PDA film reduced the XPS signal intensity of the TiO_2 substrate.[19] Figure 1D−F shows a comparison of the Ti *2p*, O *1s*, and N *1s* high-resolution spectra of the two electrode materials, respectively. The Ti *2p* peak of the TiO_2 NRs/TiO_2 QDs/PDA electrode was deconvoluted into two peaks (458.5 and 464.4 eV), representing the Ti $2p_{3/2}$ and Ti $2p_{1/2}$ states of Ti^{4+}, respectively.[20] Compared with the Ti $2p_{3/2}$ and Ti $2p_{1/2}$ peaks in the spectrum of the TiO_2 NRs/TiO_2 QDs, those in the spectrum of the TiO_2 NRs/TiO_2 QDs/PDA electrode were less intense and shifted to the direction of low binding energy. The O 1*s* peak (Figure 1E) of the TiO_2 NRs/TiO_2 QDs electrode was deconvoluted into two peaks at 530.0 and 531.4 eV (Figure S1A), corresponding to O in the crystal lattice (Ti−O−Ti) and O in Ti−OH bonds, respectively.[21] After the PDA was loaded, the O 1*s* peaks of the Ti−O−Ti and Ti−OH bonds were shifted 0.1 eV to the direction of low binding energy and a new peak appeared at 532.6 eV (Figure S1B), corresponding to the O in associative C−O/C═O in the PDA layer.[22] Compared with the O 1*s* spectrum ratio of Ti−hydroxyl/Ti−O bonds in the spectrum of the TiO_2 NRs/

https://doi.org/10.1021/acs.langmuir.1c02741
Langmuir 2022, 38, 751−761

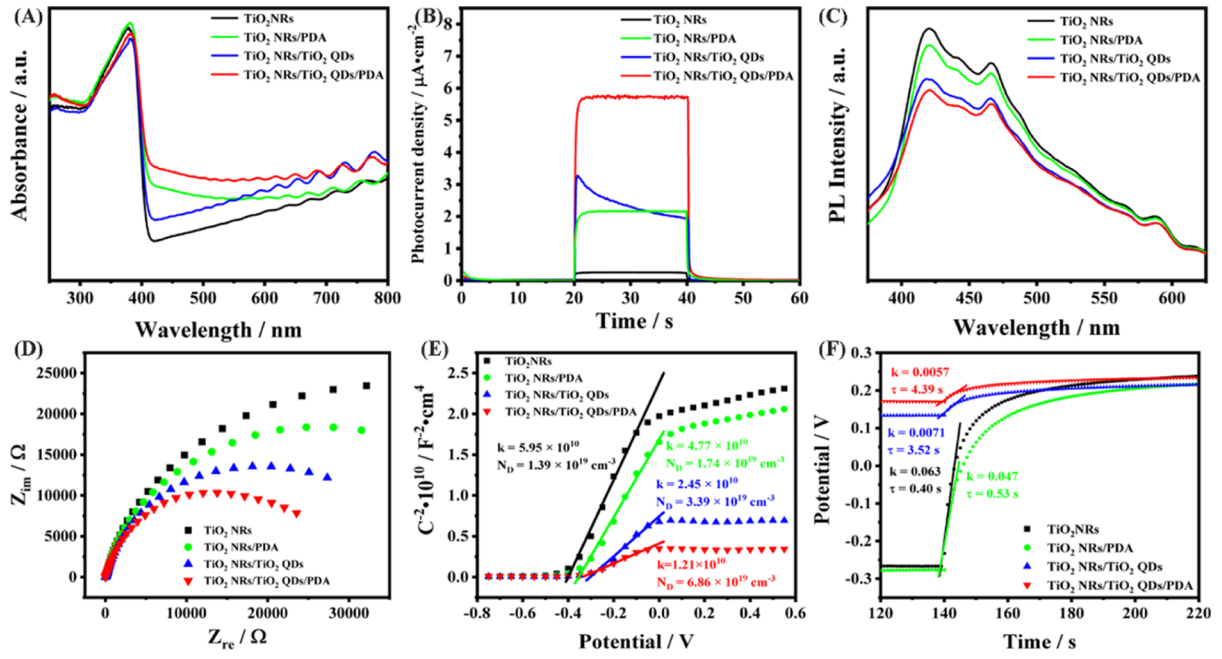

Figure 4. (A) UV−visible diffuse-reflection spectra, (B) photoelectric response when irradiated with light with a wavelength >420 nm, (C) PL spectra, (D) electrochemical impedance spectroscopy measurements, (E) M−S spectra, and (F) open-circuit potential response of TiO_2 NRs, TiO_2 NRs/TiO_2 QDs, TiO_2 NRs/PDA, and TiO_2 NRs/TiO_2 QDs/PDA electrodes.

TiO_2 QDs electrode, that in the spectrum of the TiO_2 NRs/TiO_2 QDs/PDA clearly increased, indicating that the PDA molecules might have reduced the number of oxygen vacancies by bonding well to the TiO_2 NRs/TiO_2 QDs.[23] The N 1*s* peak (Figure 1F) at 400.4 eV is attributed to the dopamine terminal group NH_3^+, indicating that the dopamine-coated TiO_2 NRs/TiO_2 QDs/PDA electrode was successfully prepared after photopolymerization.[24]

To characterize the changes in the surface morphology of the electrode materials, atomic force microscopy (AFM) was used to observe the roughness and surface morphology of each electrode material. The AFM two-dimensional (2D), three-dimensional (3D), and height profile images of each electrode material are presented in Figure 2. The average roughness (R_a) was defined as the arithmetic average of the absolute value of the surface height deviations measured from the center plane.[25] As evident in Figure 2A−C, the uneven height between the prepared NRs led to a high roughness of the TiO_2 NRs. After the TiO_2 QDs and PDA were sequentially loaded, R_a gradually decreased. The TiO_2 QDs were small particles; due to the higher chemical potential, TiO_2 QDs prefer to grow on the indentation of the nanotube, which could improve the uneven morphology of TiO_2 NRs (Figure 2D−F). Therefore, R_a of the material did not dramatically change after the TiO_2 QDs were loaded. After the PDA was loaded, R_a of the composite material was substantially reduced, indicating that photopolymerization could potentially enable the polymer film material to grow uniformly anywhere on the electrode surface (Figure 2G−I).[26] The aforementioned data all indicate that PDA was evenly loaded onto the electrode surface.

To characterize the change in morphology of the electrode materials before and after loading and explore the loaded states of the TiO_2 QDs and PDA, scanning electron microscopy (SEM) was used to observe the materials prepared in this work. Figure 3A shows an SEM image of typical TiO_2 NRs that exhibits uniform hydrothermal growth on the FTO glass substrates. The average width of the NRs was ∼120 nm, and the surface was smooth and wrinkle-free. Figure 3B shows an SEM image of the TiO_2 NRs/TiO_2 QDs. Compared with the image of the TiO_2 NRs, that of the TiO_2 NRs/TiO_2 QDs shows numerous nanoparticles on top of the TiO_2 NRs, indicating that the TiO_2 QDs were successfully loaded onto the TiO_2 NRs. However, the large amount of TiO_2 QDs loaded onto the surface of the TiO_2 NRs will result in a disordered electron-transport path, which will substantially increase the electron−hole recombination rate.[12] Therefore, the use of the nanomodified material was extremely important. As shown in Figure 3C, as a result of photopolymerization, the PDA film uniformly covered the electrode surface. The cross-sectional view of the electrode material (Figure S2A−C) also shows the successful loading of PDA onto the TiO_2 NRs. The introduction of PDA could not only control the electron transmission path of the TiO_2 QDs but also introduce reactive groups to combine with Ti-5C to form a coupled conjugate structure and construct an efficient electron transmission path.[27]

To obtain additional details of the structure of the electrode materials, the specific structure of each substance was observed more intuitively and transmission electron microscopy (TEM) was used to characterize the microstructure of the materials. Figure 3D shows a typical TEM image of rutile TiO_2 NRs. The width of the NRs was ∼120 nm, which is consistent with the SEM observations. The lattice fringes (Figure 3G) show a lattice spacing of 0.32 nm, corresponding to the (110) planes of rutile TiO_2.[16] Figure 3E shows TEM images of the TiO_2 NRs/TiO_2 QDs, where the TiO_2 QDs are clearly distributed on the surface of the NRs. To explore the molecular composition and specific morphology of the TiO_2 QDs, EDS and TEM analyses of the TiO_2 QDs powder were carried out. As shown in Figure S3, the TiO_2 QDs consisted of a titanium oxide compound (the Cu and C peaks are attributed to the instrument). The low-resolution TEM images of the TiO_2

https://doi.org/10.1021/acs.langmuir.1c02741
Langmuir 2022, 38, 751−761

QDs (Figure S4A,B) show the TiO_2 QDs distributed in the granular form, confirming the SEM results. The HRTEM images of the TiO_2 QDs (Figure S4C,D) show that the TiO_2 QDs exhibit excellent crystallinity and that the lattice fringes exhibit a lattice spacing of 0.35 nm, corresponding to the (101) planes of anatase TiO_2.[28] Consistent with the aforementioned results, lattice spacings of 0.32 and 0.35 nm are observed in the HRTEM images of TiO_2 NRs/TiO_2 QDs (Figure 3H), corresponding to the (110) planes of rutile TiO_2 and the (101) planes of anatase TiO_2, respectively. Figure 3F shows TEM images of the TiO_2 NRs/TiO_2 QDs/PDA. The TiO_2 NRs and TiO_2 QDs were wrapped in a PDA film, and the TiO_2 QDs were distributed around the NRs. This structure could be used to construct an efficient electron-transport interface and greatly improve the separation efficiency of photoelectrons and holes generated by the TiO_2 QDs.[27] HRTEM images of the TiO_2 NRs/TiO_2 QDs/PDA (Figure 3I) show that the TiO_2 NRs were coated with a uniform PDA film 20−30 nm thick. The elemental mapping analysis of a single NR in the TiO_2 NRs/TiO_2 QDs/PDA electrode is shown in Figure 3J. The matrix of the electrode was composed of Ti and O, and N was evenly distributed on the surface. These results showed that dopamine was uniformly loaded onto the electrode surface. The selected-area electron diffraction (SAED) pattern of the TiO_2 NRs (Figure 3K) shows periodic spots, corresponding to the (110) planes and the (111) planes of rutile TiO_2, respectively. This indicates that the TiO_2 NRs prepared in the present work were rutile TiO_2 single crystals. The SAED pattern of the TiO_2 NRs/TiO_2 QDs (Figure 3L) shows superior crystallinity, revealed some extra diffraction spots in addition to the (110) planes of rutile TiO_2, corresponding to the (101) planes of anatase TiO_2. These results indicated that the TiO_2 NRs/TiO_2 QDs electrode loaded with TiO_2 QDs was successfully obtained.

PEC Characterization of TiO_2 NRs/TiO_2 QDs/PDA Electrode. To explore the light absorption intensity of the electrode in the visible region and use it to demonstrate the effectiveness of the fabricated electrode, UV−visible diffuse-reflectance spectra were recorded for the TiO_2 NRs, TiO_2 NRs/TiO_2 QDs, TiO_2 NRs/PDA, and TiO_2 NRs/TiO_2 QDs/PDA electrodes (Figure 4A), and the band gap of each electrode was obtained using the Kubelka−Munk function (Figure S5). Compared with the light absorption of the TiO_2 NRs electrode, that of the TiO_2 NRs/TiO_2 QDs electrode in the visible-light range was substantially enhanced. On the one hand, the rutile phase of the TiO_2 NRs and anatase phase of the TiO_2 QDs could form a heterojunction to enhance light absorption. On the other hand, the quantum effect of the TiO_2 QDs could enhance the absorption of the electrode in the visible region. However, when the TiO_2 QDs were loaded onto the TiO_2 NRs, the absorption band edge of the electrode was not changed. PDA exhibits strong absorption in the visible-light region; thus, after the PDA was loaded, the absorption intensity of the electrode in the visible-light region was further improved. In addition, PDA is an organic semiconductor, and its loading substantially shifted the absorption band edge of the electrode because of coupling of the semiconductor levels.[17]

A series of electrochemical tests were conducted to determine the PEC performance of the TiO_2 NRs, TiO_2 NRs/TiO_2 QDs, TiO_2 NRs/PDA, and TiO_2 NRs/TiO_2 QDs/PDA electrodes under visible light. Figure 4B shows the transient photocurrent density *versus* time plots for each electrode at 0.4 V *versus* Ag/AgCl under visible light at wavelengths >420 nm with 20 s light ON/OFF cycles. The photocurrent response of the TiO_2 NRs under visible light was very weak, indicating that TiO_2 could not be excited by visible light. After the TiO_2 QDs were introduced, due to the formation of heterojunction and the quantum effect of the TiO_2 QDs, the photoelectric response of the electrode under visible light was substantially enhanced. However, the photoelectrons generated by the TiO_2 QDs were disordered in the transmission process, which greatly increased the photoelectron−hole recombination efficiency. Therefore, the photoelectric performance of the electrode decreased rapidly (Figure S6). PDA exhibits strong absorption in the visible region;[29] thus, the introduction of PDA improved the photocurrent intensity of TiO_2 under visible light to a certain extent (approximately tenfold). When the TiO_2 QDs and PDA were simultaneously loaded onto the electrodes, the TiO_2 QDs and PDA could build an efficient electronic transmission path and the TiO_2 QDs could compensate for the bulk defects between the PDA and the TiO_2 NRs; thus, the photocurrent response of the TiO_2 NRs/TiO_2 QDs/PDA electrode was improved by a factor of approximately 18, thereby demonstrating that the TiO_2 QDs and PDA could synergistically sensitize the TiO_2 NRs.

In order to characterize the effect of each component on the photoelectron−hole separation efficiency and on the charge-transfer resistance of the electrode, each electrode was characterized using photoluminescence (PL) and electrochemical impedance spectroscopy measurements. As shown in Figure 4C, the emission intensity of the TiO_2 NRs decreased after the TiO_2 QDs and PDA were introduced onto the electrode, indicating that the TiO_2 QDs and PDA could effectively reduce the recombination rate of photoelectrons and holes. As shown in Figure 4D, under visible-light irradiation, upon introduction of the TiO_2 QDs and PDA, the semicircle radius in the Nyquist plot of the material gradually decreases. In the same frequency range, the TiO_2 NRs/TiO_2 QDs/PDA electrode exhibited a smaller semicircle radius, which means that it exhibited a higher charge-transfer efficiency. The reduction in the recombination rate of photoelectrons and holes and the increase in charge transfer efficiency are all due to the construction of efficient electron transport paths.

To better understand the electron transfer mechanism of the electrodes, they were characterized using the Mott−Schottky (M−S) test and the open circuit potential (OCP) test. Capacitance measurements at the electrode/electrolyte interface were conducted to generate M−S curves. As shown in Figure 4E, all the curves had a positive slope, explaining the n-type semiconductor behavior of all the electrodes. Upon the introduction of TiO_2 QDs and PDA, the slope of M−S curves of the electrodes gradually decreased. The carrier density (N_D) of the electrode was calculated from the slope of the M−S curves using the following equation (eq 1)[30]

$$\frac{1}{C^2} = \frac{2}{N_D e \varepsilon_0 \varepsilon}\left[(U_S - U_{FB}) - \frac{k_B T}{e}\right] \quad (1)$$

where C is the space−charge capacitance in the semiconductors; e is the fundamental charge; ε and ε_0 is the relative permittivity and permittivity of vacuum in the semiconductor, respectively; U_S and U_{FB} is the applied potential and the fiat band potential in the semiconductor,

https://doi.org/10.1021/acs.langmuir.1c02741
Langmuir 2022, 38, 751−761

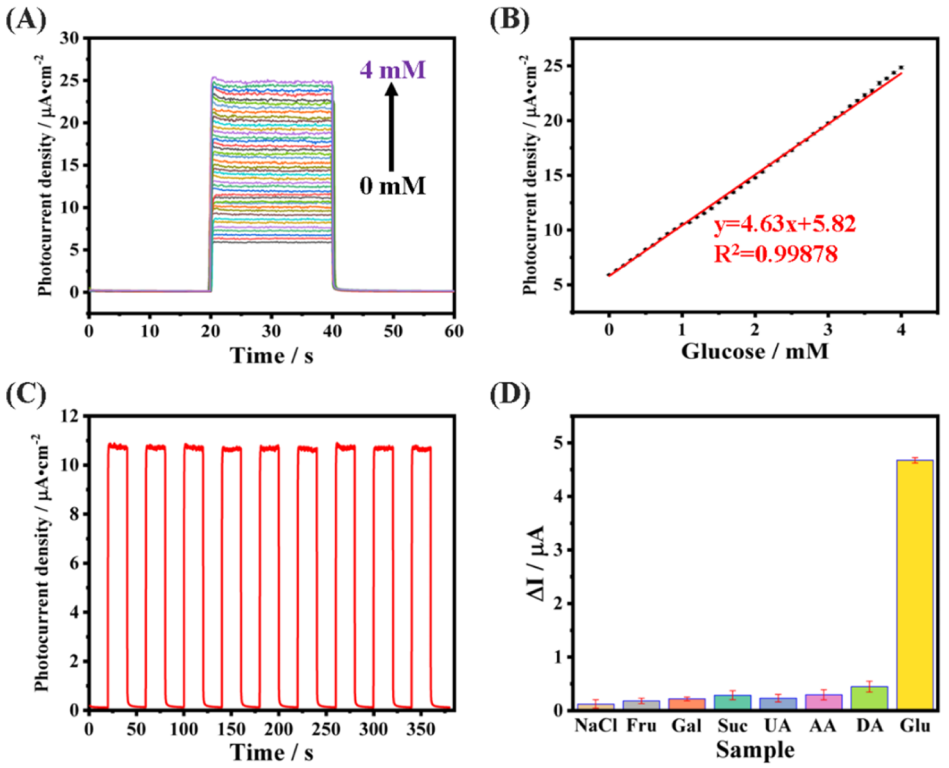

Figure 5. Under irradiation by light with a wavelength >420 nm, the (A) photocurrent response and (B) calibration curve for the TiO_2 NRs/TiO_2 QDs/PDA/GOx biosensor in 0.1 M PBS (pH = 7.4) electrolyte at different concentrations of glucose from 0 to 4 mM, (C) repeatability test at 1 mM glucose, and (D) characterization of the anti-interference performance of the electrode. The experiments were conducted in 0.1 M PBS (pH 7.4) at concentrations of 0.1 mM sodium chloride (NaCl), fructose (Fru), galactose (Gal), sucrose (Suc), uric acid (UA), ascorbic acid (AA), and dopamine (DA) in the presence of 1 mM glucose.

respectively; k_B is the Boltzmann constant; and T is the temperature. The value of N_D was calculated using eq 2:[30]

$$N_D = -\left(\frac{2}{e\varepsilon_0\varepsilon}\right)\left[\frac{d\left(\frac{1}{C^2}\right)}{d(U_S)}\right]^{-1} \quad (2)$$

where $e = 1.6 \times 10^{-19}$ C; $\varepsilon_0 = 8.86 \times 10^{-14}$ F/cm; and $\varepsilon = 170$ for rutile TiO_2.[31] The calculated N_D was 1.39×10^{-19}, 1.74×10^{-19}, 3.39×10^{-19}, and 6.86×10^{-19} cm^{-3} for the TiO_2 NRs, TiO_2 NRs PDA, TiO_2 NRs/TiO_2 QDs, and TiO_2 NRs/TiO_2 QDs/PDA electrode, respectively. These values are attributed to the introduction of TiO_2 QDs and PDA, improving the electric conductivity and accelerating the electron transfer. The results of OCP measurements with the electrodes are shown in Figure 4F, and the photoelectron lifetime was estimated on the basis of the following equation (eq 3)[30]

$$\tau = \frac{k_B T}{e}\left[\frac{dV_{OC}}{dt}\right]^{-1} \quad (3)$$

where τ is the electron lifetime and V_{OC} is the open-circuit voltage at time t. The TiO_2 NRs/TiO_2 QDs/PDA electrode displayed a longer carrier lifetime than the other electrodes, which showed high PEC performance. In general, the TiO_2 NRs/TiO_2 QDs/PDA electrode exhibited extremely high charge separation efficiency that directly benefited from the interaction among the TiO_2 NRs, TiO_2 QDs, and the PDA.

Characterization of the Sensing Performance of a TiO_2 NRs/TiO_2 QDs/PDA/GOx Biosensor. Because of its excellent photoelectric properties under visible light, the TiO_2 NRs/TiO_2 QDs/PDA electrode was used as the main photoactive substrate for PEC enzyme sensing and detection. The sensor performance of the electrode material was determined using a series of glucose tests, in which GOx plays a selective role. The parameters used to evaluate the performance of the biosensors were mainly sensitivity, linear range, and limit of detection (LOD). Figure 5A shows the photoelectric response of the TiO_2 NRs/TiO_2 QDs/PDA/GOx biosensor to different glucose concentrations under constant stirring and under irradiation with >420 nm light. GOx shows strong specificity toward oxidation of glucose, and then, when glucose was present in the PBS electrolyte solution, GOx gradually oxidized glucose into gluconic acid and H_2O_2, generating $FADH_2$ (eqs 4 and 5). The holes in the TiO_2 NRs/TiO_2 QDs/PDA electrode could capture the enzymatic products for redox reactions and generate a photocurrent. When the glucose concentration was varied, different electrical signals were generated. Detection of the electrical signals enabled the detection of biological signals. The linear regression equation for the photocurrent is represented as photocurrent (μA) = 4.63[Glu] (mM) + 5.82 (R^2 = 0.99878) (Figure 5B). In summary, the TiO_2 NRs/TiO_2 QDs/PDA/GOx biosensor showed a broad linear range from 0.1 to 4.0 mM, a high sensitivity of 4.63 μA mM^{-1} cm^{-2}, and a base LOD of 8.16 μM [signal-to-noise ratio (S/N) = 3].

$$GOx(FAD) + glucose \rightarrow GOx(FADH_2) + gluconic\ acid \quad (4)$$

$$GOx(FADH_2) + O_2 \rightarrow GOx(FAD) + H_2O_2 \quad (5)$$

https://doi.org/10.1021/acs.langmuir.1c02741
Langmuir 2022, 38, 751−761

To more clearly show the advantages of the TiO_2 NRs/TiO_2 QDs/PDA/GOx biosensors, identical glucose tests were conducted using other electrodes. The PEC $I-t$ curves for the TiO_2 NRs/GOx, TiO_2 NRs/PDA/GOx, TiO_2 NRs/TiO_2 QDs/GOx, TiO_2 NRs/TiO_2 QDs/PDA, and TiO_2 NRs/TiO_2 QDs/PDA/FAD sensors under irradiation with >420 nm light and in the presence of glucose at various concentrations are shown in Figure S7−S11. As shown in Figure S7, the response of the TiO_2 NRs/GOx biosensor was linear in the concentration range of 0.2−1.0 mM and its sensing performance was poor. This poor performance is attributed to TiO_2 exhibiting weak absorption of visible light and relatively poor biocompatibility. As shown in Figure S8, after the PDA was introduced, the TiO_2 NRs/PDA/GOx biosensor exhibited a linear response in the range of 0.2−2.4 mM, and its sensitivity decreased to 2.80 $\mu A\ mM^{-1}\ cm^{-2}$, which is 39.52% lower than that of TiO_2 NRs/TiO_2 QDs/PDA/GOx biosensors. The existing PDA reduces the electron−hole recombination rate of TiO_2 NRs to a certain extent and enhances the photoelectric response of the TiO_2 NRs; these effects, combined with the better biocompatibility of PDA, were responsible for the broader linear range of the TiO_2 NRs/PDA/GOx biosensor compared with that of the TiO_2 NRs/GOx biosensor. As shown in Figure S9, after the TiO_2 QDs were introduced, the heterojunctions enhanced the photoelectric response of the TiO_2 NRs but the transmission process of photoelectrons was disordered, resulting in poor sensitivity and a low LOD of the TiO_2 NRs/TiO_2 QDs/GOx biosensor. As shown in Figure S10, the response of the TiO_2 NRs/TiO_2 QDs/PDA biosensor was linear in the concentration range of 0.1−1.7 mM and its sensing performance was poor, and so, the presence of enzymes is necessary. As shown in Figure S11, the response of the TiO_2 NRs/TiO_2 QDs/PDA/FAD sensor was linear in the concentration range of 0.1−4.0 mM and with a sensitivity of 4.95 $\mu A\ mM^{-1}\ cm^{-2}$. The results obtained are similar to the results of the TiO_2 NRs/TiO_2 QDs/PDA/GOx biosensor, which proved that the active sites of GOx on the electrode could be regarded as the catalytic active center of the glucose enzyme sensor and perform catalytic reactions by itself in this work.[32]

Scheme 2 shows the sensing mechanism of the TiO_2 NRs/TiO_2 QDs/PDA/GOx biosensor. PDA could absorb the energy in the photon and induce a $\pi-\pi^*$ transition under visible light. The excited-state electrons transition from the highest occupied molecular orbital (HOMO, 2.501 eV *vs* NHR) of PDA to the lowest unoccupied molecular orbital (LUMO, −1.468 eV *vs* NHR).[33] The conduction-band potential (E_{CB}) values of the TiO_2 QDs and rutile TiO_2 were approximately −0.26 and −0.05 eV (*vs* NHR),[34,35] respectively; thus, a photoelectron in the HOMO of the PDA will first metastasize to the conduction band of the TiO_2 QDs, then metastasize to the conduction band of the TiO_2 NRs, and finally metastasize to the FTO substrate. In this process, TiO_2 QDs could provide more carriers and a higher charge-transfer efficiency and inhibit the recombination of photoelectrons and holes, thereby improving the PEC performance of the material. The holes generated in PDA were transferred to GOx, which promoted oxidation of glucose to gluconic acid by GOx, and the presence of PDA could effectively avoid enzyme inactivation and improve the biocompatibility of the electrode. Moreover, the improved sensing performance of the electrode is attributable to the coupling effect between the TiO_2 QDs and PDA, which form an electron transmission channel, and to the TiO_2 QDs compensating for the bulk defect of the TiO_2 NRs, further improving the photoelectron transfer efficiency of the electrode. The mechanism proposed in the preceding discussion provides a basis for the development of a steady PEC glucose biosensor based on detection under visible light.

The stability of the TiO_2 NRs/TiO_2 QDs/PDA/GOx biosensor was demonstrated by nine cycles of intermittent light radiation in the presence of 1 mM glucose. As shown in Figure 5C, after nine cycles, the photocurrent of the TiO_2 NRs/TiO_2 QDs/PDA/GOx biosensor changed only slightly, indicating good stability. The specificity of the TiO_2 NRs/TiO_2 QDs/PDA/GOx biosensor was verified by testing the effects of several components of human blood (*e.g.*, sodium chloride, Fru, Gal, Suc, UA, AA, and DA) on the sensor's glucose detection performance. GOx consisted of a protein shell and FAD. In this structure, protein was used to identify the substrate and FAD was used as catalytic active sites. When glucose is present, it could be captured by the protein shell and oxidized by FAD in GOx, which ensured the selectivity of the reaction. As shown in Figure 5D, after the interferants were added, the TiO_2 NRs/TiO_2 QDs/PDA/GOx biosensor maintained a high selectivity toward glucose, indicating that the biosensor has excellent anti-interference performance.

In addition, to further comprehend the performance of TiO_2 NRs/TiO_2 QDs/PDA/GOx biosensors in real human serum samples (provided by Hainan Medical University), $I-t$ measurement of glucose was performed in serum diluted with 0.1 M PBS. Different concentrations of glucose solutions were added to the diluted human serum, and the precision of the recovery test was assessed from five concentration gradients. As shown in Table S1, the test results show that the recovery of the TiO_2 NRs/TiO_2 QDs/PDA/GOx biosensors is between 97.64 and 100.97%. This shows that our reported TiO_2 NRs/TiO_2 QDs/PDA/GOx biosensor can be used to determine the blood glucose content in real human serum.

Finally, the performance of the TiO_2 NRs/TiO_2 QDs/PDA/GOx biosensor was compared to that of similar reported biosensors (Table 1). Benefiting from the efficient construction of electron transport channels and the high affinity of PDA for GOx, the proposed biosensor achieved satisfactory results in terms of sensitivity and LOD.

Scheme 2. Sensing Mechanism of the TiO_2 NRs/TiO_2 QDs/PDA/GOx Biosensor

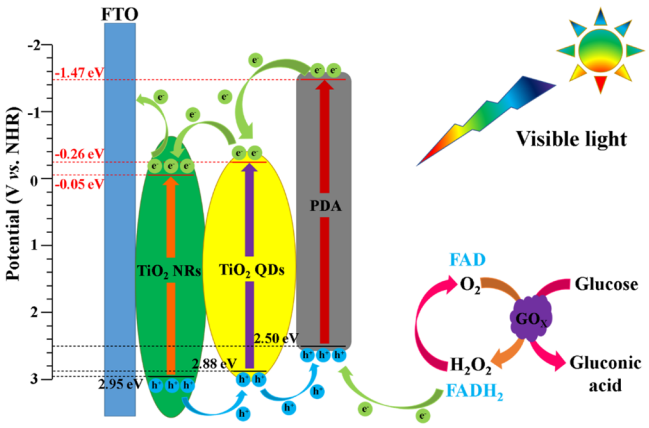

https://doi.org/10.1021/acs.langmuir.1c02741
Langmuir 2022, 38, 751−761

Table 1. Comparison of the Analytical Performance of the Proposed Glucose Biosensor with that of Previously Reported Similar Sensors

electrode	structure LOD/ μM	linear range/ mM	sensitivity/ μA mM^{-1} cm^{-2}	ref.
ITO/MoS_2-TiO_2/GOx	15.0	0.1−10	0.81	36
GOx-β-Gal@Au NPs-g−C_3N_4−MnO_2-TiO_2/ITO	0.23	0.008−2.50	1.66	37
ITO/$MTiO_2$-Au NPs-MoS_2-GOx	1.2	0.004−1.75	4.42	38
GOx/Ag_2S/SnO_2/ITO	32.4	0.1−12.2	N/A	39
ITO/NiO/CdS/GOx	10.0	0.05−7.1	0.1	40
TiO_2 NRs/PDA/GOx	12.96	0.2−2.4	2.80	this work
TiO_2 NRs/TiO_2 QDs/PDA/GOx	8.16	0.1−4.0	4.63	this work

CONCLUSIONS

A TiO_2 NRs/TiO_2 QDs/PDA electrode with enhanced visible-light response was successfully prepared as a photosensitive substrate for PEC enzyme biosensors. Finally, a TiO_2 NRs/TiO_2 QDs/PDA/GOx biosensor with excellent performance was obtained. The TiO_2 QDs and PDA jointly formed an efficient electron-transport interface, which imparted the electrode with a stronger photoelectric response under visible light. The PDA uniformly covers the surface of the electrode, not only firmly bonding the enzyme on the electrode surface but also avoiding deactivation of the enzyme *via* reaction with the strongly oxidizing holes generated in TiO_2, resulting in better sensing performance of the electrode. In addition, the presence of GOx makes the electrode highly selective to glucose. Through a series of glucose detection, the as-obtained TiO_2 NRs/TiO_2 QDs/PDA/GOx biosensor achieved a sensitivity of 4.63 μA mM^{-1} cm^{-2}, a linear response range of 0.1−4 mM, and an LOD of 8.16 μM (S/N = 3). Thus, the proposed design provides a feasible route for the development of future energy-saving, practical, and user-friendly PEC enzyme biosensors.

ASSOCIATED CONTENT

Supporting Information

The Supporting Information is available free of charge at https://pubs.acs.org/doi/10.1021/acs.langmuir.1c02741.

Materials and reagents, characterization methods, PEC measurement methods, O *1s* high-resolution XPS spectra, SEM cross-sectional images, EDS spectrum of the TiO_2 NRs/TiO_2 QDs electrode, TEM images of the TiO_2 NRs/TiO_2 QDs electrode, band gap width diagram, photoelectric response curves of the TiO_2 NRs/TiO_2 QDs electrode, photocurrent−time density response of TiO_2 NRs/GOx biosensors, TiO_2 NRs/PDA/GOx biosensors, TiO_2 NRs/TiO_2 QDs/GOx biosensors, TiO_2 NRs/TiO_2 QDs/PDA biosensors, and TiO_2 NRs/TiO_2 QDs/PDA/FAD sensors, and assay of glucose in human serum samples (PDF)

AUTHOR INFORMATION

Corresponding Authors

Delun Chen − *State Key Laboratory of Marine Resource Utilization in South China Sea, College of Materials Science and Engineering, Hainan University, Haikou 570228, China*; Email: chendelun2014@163.com

Qiang Wu − *Department of Clinical Laboratory of the Second Affiliated Hospital, School of Tropical Medicine and Laboratory Medicine, Key Laboratory of Emergency and Trauma of Ministry of Education, Research Unit of Island Emergency Medicine, Chinese Academy of Medical Sciences (No. 2019RU013), Hainan Medical University, Haikou 571199, China*; orcid.org/0000-0003-3922-5189; Email: wuqiang001001@aliyun.com

Authors

Jinxin Ma − *State Key Laboratory of Marine Resource Utilization in South China Sea, College of Materials Science and Engineering, Hainan University, Haikou 570228, China*

Miaomiao Zhang − *State Key Laboratory of Marine Resource Utilization in South China Sea, College of Materials Science and Engineering, Hainan University, Haikou 570228, China*

Wen Su − *State Key Laboratory of Marine Resource Utilization in South China Sea, College of Materials Science and Engineering, Hainan University, Haikou 570228, China*

Baiqiang Wu − *State Key Laboratory of Marine Resource Utilization in South China Sea, College of Materials Science and Engineering, Hainan University, Haikou 570228, China*

Zhuo Yang − *State Key Laboratory of Marine Resource Utilization in South China Sea, College of Materials Science and Engineering, Hainan University, Haikou 570228, China*

Xiaohong Wang − *State Key Laboratory of Marine Resource Utilization in South China Sea, College of Materials Science and Engineering, Hainan University, Haikou 570228, China*

Bin Qiao − *Department of Clinical Laboratory of the Second Affiliated Hospital, School of Tropical Medicine and Laboratory Medicine, Key Laboratory of Emergency and Trauma of Ministry of Education, Research Unit of Island Emergency Medicine, Chinese Academy of Medical Sciences (No. 2019RU013), Hainan Medical University, Haikou 571199, China*

Hua Pei − *Department of Clinical Laboratory of the Second Affiliated Hospital, School of Tropical Medicine and Laboratory Medicine, Key Laboratory of Emergency and Trauma of Ministry of Education, Research Unit of Island Emergency Medicine, Chinese Academy of Medical Sciences (No. 2019RU013), Hainan Medical University, Haikou 571199, China*

Jinchun Tu − *State Key Laboratory of Marine Resource Utilization in South China Sea, College of Materials Science and Engineering, Hainan University, Haikou 570228, China*; orcid.org/0000-0001-8793-4727

Complete contact information is available at: https://pubs.acs.org/10.1021/acs.langmuir.1c02741

Notes

The authors declare no competing financial interest.

ACKNOWLEDGMENTS

We gratefully acknowledge project supported by the Finance Science and Technology Project of Hainan Province (nos. 2019RC114, 2019RC221, 820RC647, ZDYF2021SHFZ068, and ZDKJ2021029), Hainan Province Clinical Medical Center, the National Natural Science Foundation of China (nos. 51762012, 51862006, 81860373, 81902154, and 82060386), CAMS Innovation Fund for Medical Sciences (no. 2019-I2M-

5-023), and Key Laboratory Open Project Fund of Emergency and Trauma of Ministry of Education (no. KLET-202008).

REFERENCES

(1) Hou, T.; Zhang, L.; Sun, X.; Li, F. Biphasic photoelectrochemical sensing strategy based on in situ formation of CdS quantum dots for highly sensitive detection of acetylcholinesterase activity and inhibition. *Biosens. Bioelectron.* **2016**, *75*, 359−364.
(2) Hou, T.; Xu, N.; Wang, W.; Ge, L.; Li, F. Truly Immobilization-Free Diffusivity-Mediated Photoelectrochemical Biosensing Strategy for Facile and Highly Sensitive MicroRNA Assay. *Anal. Chem.* **2018**, *90*, 9591−9597.
(3) Zhao, S.; Völkner, J.; Riedel, M.; Witte, G.; Yue, Z.; Lisdat, F.; Parak, W. J. Multiplexed Readout of Enzymatic Reactions by Means of Laterally Resolved Illumination of Quantum Dot Electrodes. *ACS Appl. Mater. Interfaces* **2019**, *11*, 21830−21839.
(4) del Barrio, M.; Luna-López, G.; Pita, M. Enhancement of Biosensors by Implementing Photoelectrochemical Processes. *Sensors* **2020**, *20*, 3281.
(5) Qadir, M.; Li, Y.; Biesiekierski, A.; Wen, C. Surface Characterization and Biocompatibility of Hydroxyapatite Coating on Anodized TiO_2 Nanotubes via PVD Magnetron Sputtering. *Langmuir* **2021**, *37*, 4984−4996.
(6) DeSario, P. A.; Pietron, J. J.; Dunkelberger, A.; Brintlinger, T. H.; Baturina, O.; Stroud, R. M.; Owrutsky, J. C.; Rolison, D. R. Plasmonic Aerogels as a Three-Dimensional Nanoscale Platform for Solar Fuel Photocatalysis. *Langmuir* **2017**, *33*, 9444−9454.
(7) Roy, P.; Kim, D.; Lee, K.; Spiecker, E.; Schmuki, P. TiO_2 nanotubes and their application in dye-sensitized solar cells. *Nanoscale* **2010**, *2*, 45−59.
(8) DeSario, P. A.; Pietron, J. J.; DeVantier, D. E.; Brintlinger, T. H.; Stroud, R. M.; Rolison, D. R. Plasmonic enhancement of visible-light water splitting with Au−TiO_2 composite aerogels. *Nanoscale* **2013**, *5*, 8073−8083.
(9) Chang, J.; Lv, W.; Wu, J.; Li, H.; Li, F. Simultaneous photoelectrochemical detection of dual microRNAs by capturing CdS quantum dots and methylene blue based on target-initiated strand displaced amplification. *Chin. Chem. Lett.* **2021**, *32*, 775−778.
(10) Méndez-Medrano, M. G.; Kowalska, E.; Ohtani, B.; Bahena Uribe, D.; Colbeau-Justin, C.; Rau, S.; Rodríguez-López, J. L.; Remita, H. Heterojunction of CuO nanoclusters with TiO_2 for photo-oxidation of organic compounds and for hydrogen production. *J. Chem. Phys.* **2020**, *153*, 034705.
(11) Saha, S.; Chan, Y.; Soleymani, L. Enhancing the Photo-electrochemical Response of DNA Biosensors Using Wrinkled Interfaces. *ACS Appl. Mater. Interfaces* **2018**, *10*, 31178−31185.
(12) Wang, G.; Wang, F.; Liu, S.; Li, M.; Xie, M.; Yang, Z.; Xiang, Y.; Lv, S.; Han, W. Construction of heterojuncted photocatalyst with TiO_2 quantum dots and graphene oxide nanosheets for highly efficient photocatalysis. *Scr. Mater.* **2021**, *199*, 113862.
(13) Ratanatawanate, C.; Chyao, A.; Balkus, K. J. S-Nitrosocysteine-Decorated PbS QDs/TiO_2 Nanotubes for Enhanced Production of Singlet Oxygen. *J. Am. Chem. Soc.* **2011**, *133*, 3492−3497.
(14) Li, H.; Lin, H.; Lv, W.; Gai, P.; Li, F. Equipment-free and visual detection of multiple biomarkers via an aggregation induced emission luminogen-based paper biosensor. *Biosens. Bioelectron.* **2020**, *165*, 112336.
(15) Fedorenko, V.; Damberga, D.; Grundsteins, K.; Ramanavicius, A.; Ramanavicius, S.; Coy, E.; Iatsunskyi, I.; Viter, R. Application of Polydopamine Functionalized Zinc Oxide for Glucose Biosensor Design. *Polymers* **2021**, *13*, 2918.
(16) Liu, B.; Aydil, E. S. Growth of Oriented Single-Crystalline Rutile TiO_2 Nanorods on Transparent Conducting Substrates for Dye-Sensitized Solar Cells. *J. Am. Chem. Soc.* **2009**, *131*, 3985−3990.
(17) Yan, B.; Zhuang, Y.; Jiang, Y.; Xu, W.; Chen, Y.; Tu, J.; Wang, X.; Wu, Q. Enhanced photoeletrochemical biosensing performance from rutile nanorod/anatase nanowire junction array. *Appl. Surf. Sci.* **2018**, *458*, 382−388.
(18) Schaefer, A.; Lanzilotto, V.; Cappel, U. B.; Uvdal, P.; Borg, A.; Sandell, A. Defect-Induced Water Bilayer Growth on Anatase TiO_2(101). *Langmuir* **2018**, *34*, 10856−10864.
(19) Hong, D.; Lee, H.; Kim, B. J.; Park, T.; Choi, J. Y.; Park, M.; Lee, J.; Cho, H.; Hong, S.-P.; Yang, S. H.; Jung, S. H.; Ko, S.-B.; Choi, I. S. A degradable polydopamine coating based on disulfide-exchange reaction. *Nanoscale* **2015**, *7*, 20149−20154.
(20) Mikulas, T.; Fang, Z.; Gole, J. L.; White, M. G.; Dixon, D. A. The presence of Ti(II) centers in doped nanoscale TiO_2 and TiO_2−xNx. *Chem. Phys. Lett.* **2012**, *539*−*540*, 58−63.
(21) Bahruji, H.; Bowker, M.; Davies, P. R. Influence of TiO_2 structural properties on photocatalytic hydrogen gas production. *J. Chem. Sci.* **2019**, *131*, 1.
(22) Li, X.; Raza, S.; Liu, C. Enhanced photo-catalytic efficiency through dual-functional ZIF based materials: Fabrication and application as a degradation of organic dyes. *J. Taiwan Inst. Chem. Eng.* **2021**, *120*, 368−380.
(23) Zhang, Z.; Wang, Y.; Li, T.; Ma, P.; Zhang, X.; Xia, B.; Chen, M.; Du, M.; Dong, W. High-Performance Polylactic Acid Materials Enabled by TiO_2−Polydopamine Hybrid Nanoparticles. *Ind. Eng. Chem. Res.* **2021**, *60*, 3999−4008.
(24) Beckford, S.; Zou, M. Wear resistant PTFE thin film enabled by a polydopamine adhesive layer. *Appl. Surf. Sci.* **2014**, *292*, 350−356.
(25) Rožić, L. J.; Petrovic, S.; Radic, N.; Stojadinovic, S.; Vasilic, R.; Stefanov, P.; Grbic, B. Fractal approach to surface roughness of TiO_2/WO_3 coatings formed by plasma electrolytic oxidation process. *Thin Solid Films* **2013**, *539*, 112−116.
(26) Guo, Z.; Wang, G.; Fu, H.; Wang, P.; Liao, J.; Wang, A. Photocatalytic degradation of methylene blue by a cocatalytic PDA/TiO_2 electrode produced by photoelectric polymerization. *RSC Adv.* **2020**, *10*, 26133−26141.
(27) Zhang, N.; Ruan, Y.-F.; Ma, Z.-Y.; Zhao, W.-W.; Xu, J.-J.; Chen, H.-Y. Simultaneous photoelectrochemical and visualized immuno-assay of β-human chorionic gonadotrophin. *Biosens. Bioelectron.* **2016**, *85*, 294−299.
(28) Djokić, V. R.; Marinković, A. D.; Petrović, R. D.; Ersen, O.; Zafeiratos, S.; Mitrić, M.; Ophus, C.; Radmilović, V. R.; Janaćković, D. T. Highly Active Rutile TiO2 Nanocrystalline Photocatalysts. *ACS Appl. Mater. Interfaces* **2020**, *12*, 33058−33068.
(29) Vega, M.; Martín del delín, E. M.; Pérez, M.; Pecharromán, C.; Marcelo, G. Color Engineering of Silicon Nitride Surfaces to Characterize the Polydopamine Refractive Index. *Chemphyschem* **2018**, *19*, 3418−3424.
(30) Xin, Y.; Li, Z.; Zhang, Z. Photoelectrochemical aptasensor for the sensitive and selective detection of kanamycin based on Au nanoparticle functionalized self-doped TiO_2 nanotube arrays. *Chem. Commun.* **2015**, *51*, 15498−15501.
(31) Bonkerud, J.; Zimmermann, C.; Weiser, P. M.; Vines, L.; Monakhov, E. V. On the permittivity of titanium dioxide. *Sci. Rep.* **2021**, *11*, 12443.
(32) Lv, W.; Wang, X.; Wu, J.; Li, H.; Li, F. pH and H_2O_2 dual-responsive carbon dots for biocatalytic transformation monitoring. *Chin. Chem. Lett.* **2019**, *30*, 1635−1638.
(33) Yu, F.; Chen, S.; Chen, Y.; Li, H.; Yang, L.; Chen, Y.; Yin, Y. Experimental and theoretical analysis of polymerization reaction process on the polydopamine membranes and its corrosion protection properties for 304 Stainless Steel. *J. Mol. Struct.* **2010**, *982*, 152−161.
(34) Yu, X.; Zhao, Z.; Zhang, J.; Guo, W.; Qiu, J.; Li, D.; Li, Z.; Mou, X.; Li, L.; Li, A.; Liu, H. Rutile Nanorod/Anatase Nanowire Junction Array as Both Sensor and Power Supplier for High-Performance, Self-Powered, Wireless UV Photodetector. *Small* **2016**, *12*, 2759−2767.
(35) Nguyen, V.-H.; Mousavi, M.; Ghasemi, J. B.; Le, Q. V.; Delbari, S. A.; Sabahi Namini, A.; Shahedi Asl, M.; Shokouhimehr, M.; Mohammadi, M. Novel p−n Heterojunction Nanocomposite: TiO_2 QDs/$ZnBi_2O_4$ Photocatalyst with Considerably Enhanced Photo-catalytic Activity under Visible-Light Irradiation. *J. Phys. Chem. C* **2020**, *124*, 27519−27528.

https://doi.org/10.1021/acs.langmuir.1c02741
Langmuir 2022, 38, 751−761

(36) Liu, X.; Huo, X.; Liu, P.; Tang, Y.; Xu, J.; Liu, X.; Zhou, Y. Assembly of MoS_2 nanosheet-TiO_2 nanorod heterostructure as sensor scaffold for photoelectrochemical biosensing. *Electrochim. Acta* **2017**, *242*, 327−336.
(37) Çakıroğlu, B.; Demirci, Y. C.; Gökgöz, E.; Özacar, M. A photoelectrochemical glucose and lactose biosensor consisting of gold nanoparticles, MnO_2 and g-C_3N_4 decorated TiO_2. *Sens. Actuators, B* **2019**, *282*, 282−289.
(38) Çakıroğlu, B.; Özacar, M. A Photoelectrochemical Biosensor Fabricated using Hierarchically Structured Gold Nanoparticle and MoS_2 on Tannic Acid Templated Mesoporous TiO_2. *Electroanal* **2020**, *32*, 166−177.
(39) Zhang, X.; Liu, M.; Liu, H.; Zhang, S. Low-toxic Ag_2S quantum dots for photoelectrochemical detection glucose and cancer cells. *Biosens. Bioelectron.* **2014**, *56*, 307−312.
(40) Wang, G.-L.; Liu, K.-L.; Dong, Y.-M.; Wu, X.-M.; Li, Z.-J.; Zhang, C. A new approach to light up the application of semiconductor nanomaterials for photoelectrochemical biosensors: Using self-operating photocathode as a highly selective enzyme sensor. *Biosens. Bioelectron.* **2014**, *62*, 66−72.

https://doi.org/10.1021/acs.langmuir.1c02741
Langmuir 2022, 38, 751−761